Target Identification Using Modeled Radar Cross Sections and a Coordinated Flight Model

Lisa M. Ehrman and Aaron D. Lanterman

Center for Signal and Image Processing
School of Electrical and Computer Engineering
Georgia Institute of Technology, Atlanta, GA 30332, USA

ABSTRACT

Passive radar is a rapidly emerging technology with many distinct advantages over traditional radar. Its exploitation of "illuminators of opportunity" renders it covert, as well as less expensive. Several passive radar systems, such as Lockheed Martin's Silent Sentry and John Sahr's Manastash Ridge Radar at the University of Washington, are already capable of detecting and tracking aircraft. Our goal is to enhance such systems with the addition of automatic target recognition capabilities.

We propose conducting target recognition by comparing the radar cross section (RCS) of detected targets to the simulated RCS of known targets. Since RCS is the sole parameter for identification, it is imperative that RCS be modeled accurately. This approach begins by simulating the RCS of aircraft in the target class using the Fast Illinois Solver Code (FISC). These FISC results are then compiled into a database, providing aircraft RCS from a variety of incident and observed angles. Since RCS is highly aspect dependent, aircraft orientation must be known. This challenge is met with a coordinated flight model, which estimates aircraft orientation from aircraft position. To provide further accuracy, the RCS is scaled to account for propagation losses and the receiving antenna gain; these tasks are accomplished using the Advanced Refractive Effects Prediction System (AREPS) and Numerical Electromagnetic Code (NEC2), respectively. The Rician model then compares the simulated RCS of known targets to the RCS arriving at the receiver. Target identification results from this comparison.

Thus far, the results are encouraging. The algorithm is able to correctly identify aircraft in the target class with exceptional accuracy at the anticipated noise levels. Performance declines as the noise power surpasses the maximum signal power, but even then, little degradation is noted due to the use of the coordinated flight model.

Keywords: Automatic Target Recognition, Passive Radar, Coordinated Flight Model, Radar Cross Section

1. INTRODUCTION

1.1. History of the Problem

There are two parallel schools of thought prevalent in the literature regarding the recognition of fast-moving fixed-wing aircraft. The first approach proposes the creation of target images, such as two-dimensional inverse synthetic aperture radar (ISAR) images or a sequence of one-dimensional range profiles.[1] Target recognition is then conducted using these images. The alternate approach has been to bypass the creation of images and attempt recognition directly from the received data. Herman[2,3] takes this second approach to automatic target recognition (ATR), using data obtained from a passive radar system.

Although ATR has been a subject of much research, Herman's application of passive radar was innovative. Unlike traditional radar systems, passive radar systems bypass the need for dedicated transmitters by exploiting "illuminators of opportunity" such as commercial television and FM radio signals. In doing so, they are able to reap a number of benefits. Most notably, the fact that passive radar systems do not emit energy renders them covert; this is a great strategic advantage if the systems are employed by the military. Passive radar systems may also be much less expensive than traditional ones, where most of the cost is associated with the transmitter.

Additionally, many illuminators of opportunity employ low frequencies. Although passive radar systems do not inherently require these low frequencies, the allocation of bandwidth for commercial TV and FM radio

(Tel: 404-385-2548. Fax: 404-894-8363. Email: ehrman@ece.gatech.edu, lanterma@ece.gatech.edu)

implies that passive radar systems operate at lower frequencies than traditional microwave radar. As a fortunate though unintended consequence, the low-frequency signals exploited by passive radar are well-suited for ATR.[4–6] In addition to being less susceptible to inclement weather, the longer wavelengths result in target radar cross sections that vary "slowly" with small changes in the target state vector. Herman noted that the variation in radar cross section (RCS), as characterized by the number of nulls encountered as a target's aspect changes, is proportional to the electrical length of the target.[2, 3] At FM-band frequencies (100 MHz), a fighter-sized aircraft is approximately five wavelengths long. In contrast, at the X-band frequencies used by many traditional radars (10 GHz), the same aircraft would be 500 wavelengths long, making the ATR system very sensitive to small changes in target orientation.

Despite its numerous benefits, passive radar was once deemed impractical. In the mid-1980s, Griffiths and Long[7] attempted to extract range information from backscattered television signals. Plagued by the low signal-to-noise ratio resulting from the available equipment and the range ambiguity inherent in the sync pulses of an analog TV signal, their results did not seem encouraging. A decade later, Howland[8] successfully tracked targets by abandoning any attempt to directly measure range in favor of the velocity information contained in the Doppler-shifted TV carrier and the angle-of-arrival information derived from a simple two-antenna array. Exotic track initialization algorithms, combined with an extended Kalman filter, fuse the Doppler and angle-of-arrival information into Cartesian coordinate tracks.

Today, several passive radar systems are in operation. The most widely tested manifestation of this kind of technology is probably the Silent Sentry series developed by Lockheed Martin Mission Systems of Gaithersburg, MD, which can exploit both analog television and FM radio signals. Another well-known system is the Manastash Ridge Radar* developed by John Sahr at the University of Washington,[9, 10] which uses FM radio-based passive radar for atmospheric studies.

1.2. A New Approach to ATR

The primary goal of this research is to add ATR capabilities to existing passive radar systems, using RCS as the key information for classification. Since RCS is highly aspect-dependent, accurate estimation of target orientation is crucial. Herman[2, 3] met this challenge with a computationally intensive particle filter,[11] which jointly estimated target position, orientation, and target type. This paper seeks a less computationally intensive approach. The positions and velocities estimated by the existing passive radar system are considered to be "true." They are then exploited by a coordinated flight model[12] to estimate aircraft orientation.

A database of Fast Illinois Solver Code (FISC) results is created for each aircraft in the target class. This database is accessed using the aircraft orientations estimated by the coordinated flight model. This results in a set of power profiles simulating those that would arrive at the receiver if the aircraft in the target class were executing the maneuver. These profiles are then scaled for propagation losses and antenna gain of the receiver using the Advanced Refractive Effects Prediction System (AREPS) and Numerical Electromagnetic Code (NEC2), respectively. Finally, the profiles corresponding to members of the target class are compared to the profile of the actual target, resulting in target identification.

The work presented here is simulation-based. Target profiles arriving at the receiver are simulated by adding white Gaussian noise to the profile. One hundred such noisy profiles are created for each member of the target class for each scenario to create a statistically significant set of simulations. It is worth noting that the aircraft comprising the target classes are chosen based upon the availability of acceptable CAD models, rather than likelihood of occurrence near a real system. A secondary goal of this research is to model a system currently being developed by NATO/NC3A with the intent of an eventual comparison with real data. At that point, more realistic target classes will be implemented.

2. MODELING RCS

2.1. System Description

The system parameters used in this work are selected to model a passive radar demonstration currently being developed by NATO. Table 1 shows the relevant parameters for the transmitter and receiver modeled in this research. Note that the NATO system uses vertically polarized antennas.

*www-rcs.ee.washington.edu/~radar/Projects/Manastash

Table 1. Transmitter and receiver parameters.

Parameter	Transmitter	Receiver
Latitude (N)	52^o 01' 00"	52^o 06' 36"
Longitude (E)	05^o 03' 00"	04^o 19' 26"
Altitude (m ASL)	375	100
Frequency (MHz)	100	–
Peak Power (kW)	100	–
Direction	Omni-Directional	320^o

2.2. Estimating Aircraft Orientation with a Coordinated Flight Model

Given that target RCS is the sole factor used to classify the aircraft, its accurate representation is paramount. This is not a trivial task, as RCS is heavily dependent upon the incident and observed angles, which in turn are dependent upon the yaw, heading, pitch, and roll of the aircraft. Our response to this challenge implements a coordinated flight model to estimate these angles, given a set of time-correlated aircraft positions. This process is described at length in other sources,[12 13]; thus, only the results will be presented here.

Since this research is primarily concerned with fast-moving fixed-wing aircraft, yaw is always assumed to be zero. This does not imply that aircraft direction goes unmeasured; it simply means that the aircraft nose is assumed to be oriented in the direction of motion. Aircraft heading, a far more revealing parameter, is expressed as,

$$\xi = \begin{cases} 90 - \arctan(\frac{v_Y}{v_X}), x > 0 \\ 270 - \arctan(\frac{v_Y}{v_X}), x < 0 \end{cases}, \tag{1}$$

where v_X and v_Y are the x and y components of aircraft velocity. The equation of pitch also follows from the assumption that the aircraft nose is pointed in the direction of motion, and is expressed as,

$$\theta = \arctan\left(\frac{dz}{\sqrt{dx^2 + dy^2}}\right), \tag{2}$$

where (dx, dy, dz) is the difference in aircraft position in the x, y, and z directions over an incremental period of time, dt. Finally, the aircraft roll is estimated as,

$$\phi = \arctan\left(\frac{|v|^2 \cos(\theta)}{Rg}\right), \tag{3}$$

where $|v|$ is the magnitude of the aircraft velocity, R is the instantaneous radius of curvature of the aircraft turn, and g is the standard gravity at Earth's surface. At this point, we are assuming that the load factor is equal to one. That will change in future work.

The estimated aircraft orientation angles are appended to the aircraft positions, creating a supplemented flight profile. This is then used to determine the incident and observed angles, upon which RCS depends.

2.3. Modeling Target Radar Cross Section

Modeling the power profile arriving at the receiving antenna is a multi-step process. The supplemented flight profile, containing aircraft position and orientation, is used to determine the incident and observed angles at every point during the encounter. The incident and observed angles are then used to access a database of FISC results which are available for each aircraft model in the target class. A set of power profiles are created when data is extracted from the RCS database. Additional scaling is required to make these power profiles represent the signals arriving at the receiver due to the illuminated targets. Some significant factors that must be considered are propagation losses between the aircraft and antennas, and antenna gain. The propagation losses, which include effects due to multipath, are modeled using AREPS. As is likely to be the case for most

passive radar applications, the transmitting antenna exploited by the NATO system is omni-directional. Thus, the only antenna gain pattern that must be modeled corresponds to the receiver; this modeling is accomplished with NEC2. To cut down on the length of time required to execute the simulation, databases are also created for AREPS and NEC2. The overall result of this process is a power profile that is scaled to account for propagation losses and antenna gain.

The necessity of the FISC database, as well as its limitations, are worth mentioning. Ideally, the simulation process described here would run FISC for every new set of incident and observed angles. However, the lengthy run-time and massive memory requirements of FISC render this option unfeasible. A more attractive option is the creation of a database of FISC results, in which aircraft RCS is sampled sufficiently to meet the Nyquist sampling criterion. In particular, the angular sampling of the RCS should satisfy,

$$\Delta\theta \leq \frac{c}{(2f_0)(size)}, \tag{4}$$

where c is the speed of light, f_0 is the radar frequency, and $size$ is the longest dimension of the aircraft.[14] The minimum angular sampling required for each aircraft when the frequency is 100 MHz is shown in Table 2.

Table 2. Minimum angular sampling required for each aircraft in target class.

Aircraft	Longest Dimension (m)	Minimum Spacing (deg)
F-15	19.3	4.5
Falcon-20	17.1	5.0
Falcon-100	13.7	6.2
T-38	14.0	6.2

Thus, using an angular spacing of 4^o, a database of FISC runs can be created that is sufficiently full to represent the RCS of each aircraft type in the study, without aliasing. This database can be quickly accessed and allows for the creation of virtually any desired power profile.

Although the profiles simulated by FISC are sampled as sparsely as possible while avoiding aliasing, the amount of time required to create a sufficiently large database remains daunting. At this point, the database has been completed for all combinations of observed azimuths and elevations, and incident azimuths. However, the incident elevations available in the database† are currently limited to $\pm 20^o$. More sophisticated techniques will eventually be implemented to circumvent this limitation.

2.4. Modeling the Power Arriving at the Receiver

Recall that one goal of this research is to model a system currently being developed by NATO. Eventually, real power profiles may be available from the NATO receiver. Until then, it is necessary to simulate these profiles.

First, the simulation is run with the real aircraft orientations used in place of the estimated ones. These power profiles are then corrupted with additive white Gaussian noise, which acts independently on the real and imaginary parts of the signal. Along these lines, the simulated received profile is expressed as,

$$P_{SIM} = (\sqrt{P_R} + w_R)^2 + w_I^2, \tag{5}$$

where P_R is the real component of the power profile prior to being corrupted by noise, and w is zero-mean additive white Gaussian noise, which has real and imaginary components, w_R and w_I.[3] The noise power is computed in dBW using,

$$P_N = \frac{kT_0N_F}{CPI}, \tag{6}$$

†FISC requires a great deal of computational time to find the currents on the aircraft for a particular set of incident angles; however, once the model has been created for the set of incident angles, all of the possible pairs of observed angles can be computed relatively quickly. For this reason, the limited parameter in our database is the incident elevation.

where k is Boltzmann's constant, T_0 is temperature in Kelvin, N_F is the unitless noise figure, and CPI is the coherent processing interval of the system.[15] To match the NATO system, the CPI is set equal to 0.5 seconds, and T_0 is set equal to 290 K.

Selection of the noise figure, N_F, is more difficult. If the noise figure is only expected to account for thermal noise and out-of-band interference, then a conservative estimate of the noise figure in a city environment might be 30 dB. In the absence of data regarding the noise power of the NATO system, it is reasonable to use this approximation. In an attempt to be thorough and to anticipate the possibility that the NATO passive radar system, once developed, may have a different noise power, it seems prudent to sweep the noise figure over a range of values. Using this approach, it is possible to quantify system performance as a function of noise power. The noise figures used in this paper range from 30 dB to 100 dB in increments of 5 dB. Note that noise figures above 30 dB are not expected to occur in a real setting; they are merely included in this paper to demonstrate the breaking point of the algorithm.

2.5. Noise Power Due to Transmitter Interference

The noise figure accounts for thermal noise and out-of-band interference, but until now the issue of transmitter interference has not been addressed. Typically, this direct path interference manifests itself as a spike in the cross-ambiguity function. Since the transmitter's power and location are known, and since the direct path interference spike occurs along the axis with zero velocity, this spike can usually be identified and removed. The more treacherous effect of transmitter interference is that is can raise the "thumbtack" noise floor of the ambiguity function, potentially masking the target spike. To be thorough, this should also be considered when computing the noise figure.

If the ambiguity function is normalized such that the direct path spike has unit height, then the average pedestal height, or sideband power, is given by

$$P_{pedestal} = \frac{1}{B \times CPI}, \tag{7}$$

where B is the signal bandwidth, and CPI is the coherent processing interval.[16] To match the NATO system, values of 45 kHz and 0.5 seconds are used for B and CPI, respectively. If propagation losses and antenna gain are neglected, the pedestal power is 44 dBW below the direct-path spike. Since the NATO transmitter power is 50 dBW, the sideband power is 6 dBW. Propagation losses and antenna gain play a significant role, lowering the pedestal power by 95 dBW. The electronics in the receiver of the NATO system also mitigate the problem by suppressing the direct path signal by 70 dBW, which reduces the sideband power to -159 dBW. More sophisticated filters could be implemented to further reduce the noise figure, but using the specifications of the system being modeled, the effective noise figure falls between 40 and 45 dB. Thus, the effects due to transmitter interference are far more significant than those due to thermal noise and out-of-band interference.

2.6. Target Identification

The process described in Section 2.4 is repeated for each member of the target class, resulting in a set of simulated received profiles. The automatic target recognizer compares these noisy received profiles to the library of noise-free profiles. Equation 5 leads to a Rician likelihood model[3] whose probability density function is given by

$$p_x(x) = \frac{x}{\sigma_w^2} e^{\left(\frac{x^2+s^2}{2\sigma_w^2}\right)} I_0\left[\frac{xs}{\sigma_w^2}\right]. \tag{8}$$

To apply the Rician to the simulated and truth profiles, associate x with the magnitude of the received profile, and s with the magnitude of the library profile. The noise power, which equals the noise variance, is then equated with σ_w^2. If each point in time is considered an independent sample from a process, then the data loglikelihood is

$$\ln(p_x(\bar{x})) = \sum_{i=1}^{n} \ln\left(I_0\left[\frac{x_i s_i}{\sigma_w^2}\right]\right) - \left(\frac{x_i^2 + s_i^2}{2\sigma_w^2}\right). \tag{9}$$

Loglikelihoods are computed for each member of the target class; the target is identified as the member of the target class with the largest loglikelihood.[17]

3. RESULTS

Three scenarios of increasing complexity are presented to the algorithm. The locations of these three maneuvers relative to the system transmitter and receiver are shown in Figure 1.

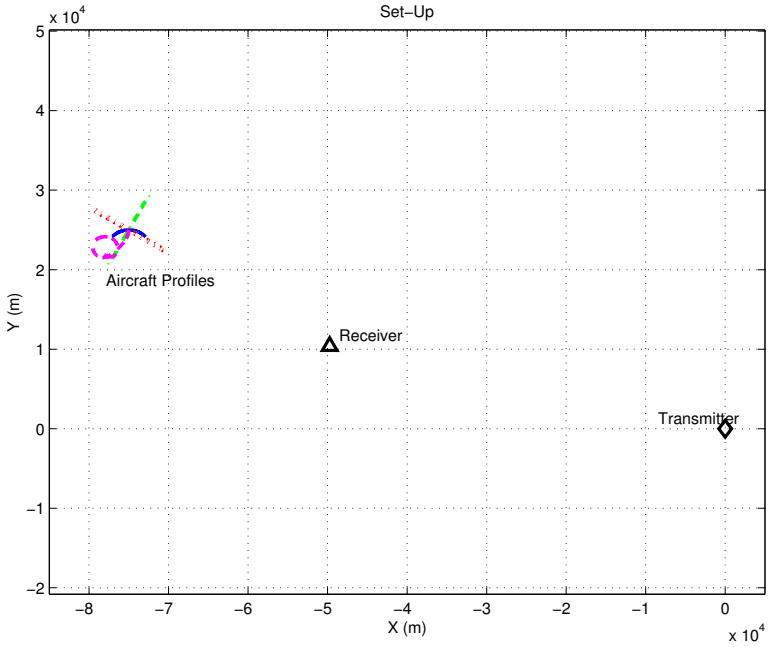

Figure 1. Maneuver locations relative to system transmitter and receiver.

The first scenario consists of a simple straight-and-level flight path. This does little to test the coordinated flight model, but gives a good indication that the remainder of the algorithm is working. To be thorough, two straight-and-level trajectories have been tested. The aircraft in the first trajectory flies away from the receiver, while the aircraft in the second trajectory flies broadside to the receiver. Notable differences in the results are observed.

The next scenario implements a constant-altitude, circular banked turn. Although this circular banked turn is not a realistic flight trajectory, it indicates that the algorithm is able to perform when the aircraft power profiles become more complex. It also provides a more strenuous test of the coordinated flight model than the straight-and-level trajectories.

Finally, a flight profile recorded on-board a maneuvering F-15 at Edwards Air Force Base[‡] is used to provide a more realistic test of the algorithm. The Edwards trajectory came complete with measured aircraft orientation, allowing a unique opportunity to quantify the performance degradation induced from having to estimate aircraft orientation. First, the algorithm is executed with the real aircraft orientation angles used in place of the ones estimated by the coordinated flight model. This serves as a baseline for comparison. Next, the simulation is run using the estimated aircraft orientation angles. Finally, a test is conducted in which the aircraft position is errantly estimated to be 300 m north and 300 m west of its actual location. This gauges performance degradation due to errors in the position estimates.

[‡]The F-15C trajectory was obtained from the Joint Helmet Cuing System, Mission JH-16, conducted by the 445th Flight Test Squadron at Edwards Air Force Base in May 2000.

3.1. Straight-and-Level Trajectory # 1

The straight-and-level trajectory used in the first scenario contains targets moving at 200 m/s with altitudes of 8000 m. The library profiles resulting from this maneuver are shown in Figure 2a. Note that the sharp dip in the profiles around 42 seconds is an artifact of the process used to model the propagation losses between the transmitter and aircraft. In this case, the AREPS profile is the source of this artifact. Although this artifact could be removed by increasing the resolution in the AREPS database, such artifacts are rare and the tradeoff between database size and accuracy must be considered.

The noise figure is swept from 30 dB to 100 dB, in increments of 5 dB, to gauge performance degradation as a function of noise power. One-hundred runs are executed using each aircraft as the true target, for each noise figure. The percentage of incorrect identifications (probability of error) obtained for each aircraft model at each noise level is shown in Figure 2b. This data is obtained from a set of Monte Carlo runs; thus the jumps in the curves are artificial and are expected to smooth out as the number of samples increase.

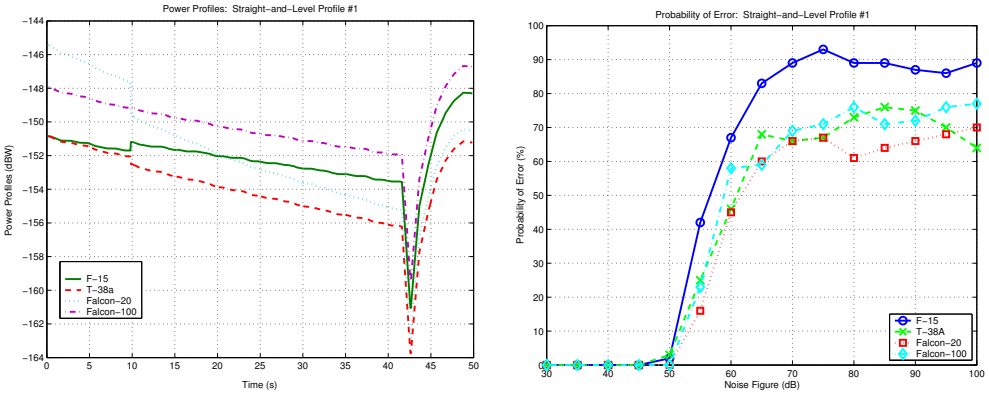

Figure 2. Straight-and-level flight profile #1: a.) power profiles (left), b.) probability of error vs. noise nigure (right).

Comparison of the probability of error plot with the plot of the power profiles provides insight into the viability of the algorithm. Figure 2a demonstrates that the algorithm performs perfectly until the noise figure reaches 50 dB. This corresponds to noise power of -151 dBW. Using the plot of the power profiles in Figure 2b, it is clear that this noise power is approximately equal to the maximum power of the signal. Thus, algorithm performance declines when the noise power surpasses the maximum signal power. It is also noteworthy that the probability of error at high noise figures, for all four aircraft, is in the ballpark of 75%. This implies that when the signal is buried in the noise, the odds of the algorithm correctly identifying an aircraft are one in four; since there are four aircraft models in the target class, this is equivalent to chance.

Confusion matrices are tabulated to provide further insight into the types of mistakes being made by the algorithm. The aircraft listed in the first column correspond to the aircraft used to create the power profile at the receiver. The aircraft listed across the top row pertain to the aircraft identified by the algorithm. The confusion matrices for this encounter, with noise figures of 50, 55, and 60 dB are shown in Tables 3 through 5.

Table 3. Confusion matrix for straight-and-level trajectory #1 with noise figure = 50 dB.

Aircraft	F-15	T-38A	Falcon-20	Falcon-100
F-15	98	1	0	1
T-38A	3	97	0	0
Falcon-20	0	0	100	0
Falcon-100	0	0	0	100

Table 4. Confusion matrix for straight-and-level trajectory #1 with noise figure = 55 dB.

Aircraft	F-15	T-38A	Falcon-20	Falcon-100
F-15	58	24	3	15
T-38A	21	75	3	1
Falcon-20	1	5	84	10
Falcon-100	14	3	6	77

Table 5. Confusion matrix for straight-and-level trajectory #1 with noise figure = 60 dB.

Aircraft	F-15	T-38A	Falcon-20	Falcon-100
F-15	33	34	13	20
T-38A	20	54	13	13
Falcon-20	10	19	55	16
Falcon-100	22	13	23	42

3.2. Straight-and-Level Trajectory # 2

The straight-and-level trajectory is then translated to a new location and rotated such that the aircraft flies broadside to the receiver. This seemingly minor change has a significant effect on the amplitude of the power profiles and, in turn, on algorithm performance. The power profiles and probability of error plots are shown in Figures 3a and 3b, respectively.

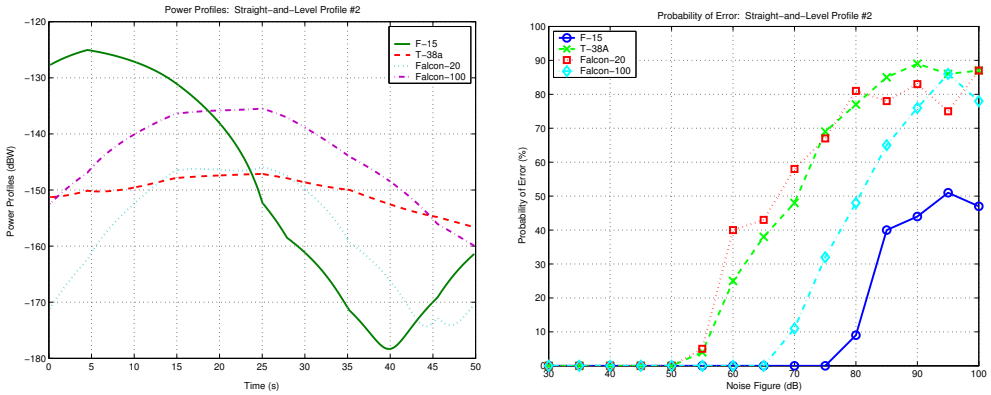

Figure 3. Straight-and-level flight profile #2: a.) power profiles (left), b.) probability of error vs. noise figure (right).

With this change in trajectory, the algorithm is able to correctly identify the aircraft at much higher noise levels. This improvement in performance corresponds to an increase in the amplitude of the power profiles. For example, the maximum signal power obtained when the F-15 executes the first straight-and-level maneuver is approximately -150 dBW; however, in the second straight-and-level maneuver, the maximum signal power due to the F-15 is -125 dBW. To surpass the maximum signal power from the F-15 in the second straight-and-level maneuver, the noise figure N_F must be greater than 75 dB. Figure 3b reveals that the algorithm does not begin to misidentify the F-15 until the noise figure is greater than 75 dB. As in the first maneuver, the algorithm is capable of correctly identifying aircraft until the noise power surpasses the maximum signal power. This pattern holds for the other aircraft models in the target class, as well. The maximum signal power from the Falcon-100 increases from -150 dBW in the first straight-and-level maneuver, to -135 dBW in the second. Similarly, the noise figure at which the algorithm begins misidentifying the Falcon-100 rises from 45 dB to 65 dB. The amplitude of the power profiles of the Falcon-20 and T-38A remains about the same, as does the algorithm's ability to identify them.

The confusion matrices for this maneuver, shown in Tables 6 through 8, reveal a dramatic pattern. Consider the first confusion matrix, for which the noise figure is 55 dB. Figure 3b demonstrates that the only aircraft misidentified by the algorithm at this noise level are the T-38A and Falcon-20. The confusion matrix reveals that the misidentification errors are limited to swapping the T-38A and Falcon-20. Neither of these aircraft are mistakenly identified as the F-15 or Falcon-100. This pattern continues in Table 7. In this case, the only aircraft not being misidentified is the F-15. As before, the T-38A, Falcon-20, and Falcon-100, though misidentified by the algorithm, are never misidentified as the F-15. This pattern implies that the algorithm's main error is to swap aircraft whose power profiles have comparable amplitude. This swapping begins to occur when the maximum signal power generated by the aircraft becomes buried in the noise.

Table 6. Confusion matrix for straight-and-level trajectory #2 with noise figure = 55 dB.

Aircraft	F-15	T-38A	Falcon-20	Falcon-100
F-15	100	0	0	0
T-38A	0	96	4	0
Falcon-20	0	5	95	0
Falcon-100	0	0	0	100

Table 7. Confusion matrix for straight-and-level trajectory #2 with noise figure = 70 dB.

Aircraft	F-15	T-38A	Falcon-20	Falcon-100
F-15	100	0	0	0
T-38A	0	52	40	8
Falcon-20	0	50	42	8
Falcon-100	0	2	9	89

Table 8. Confusion matrix for straight-and-level trajectory #2 with noise figure = 80 dB.

Aircraft	F-15	T-38A	Falcon-20	Falcon-100
F-15	91	3	0	6
T-38A	16	23	19	42
Falcon-20	15	24	19	42
Falcon-100	17	17	14	52

3.3. Bank-Turn Trajectory

The constant-altitude circular banked turn provides a more difficult test of the algorithm. In this case, the target velocity is 100 m/s, and the altitude is 8000 m. Like the straight-and-level profiles, this is an idealized maneuver, rather than one recorded during an actual flight. Unlike the straight-and-level maneuver, this trajectory requires the coordinated flight model to estimate non-zero aircraft roll. The power profiles and probability of error curves are shown in Figures 4a and 4b.

In this case, the maximum signal power is roughly -150 dBW for all four aircraft models. Thus, algorithm performance is expected to be excellent for all four aircraft until the noise figure rises above 50 dB. Figure 4b supports this claim. Also note that the probability of error curves are more tightly clustered around 75% at high noise levels than before. This is attributed to the fact that the power profiles generated by all four aircraft have comparable amplitudes. Using the pattern described in Section 3.2, the swapping errors made by the algorithm are expected to encompass all four aircraft models. The confusion matrices, shown in Tables 9 through 11, confirm this suspicion.

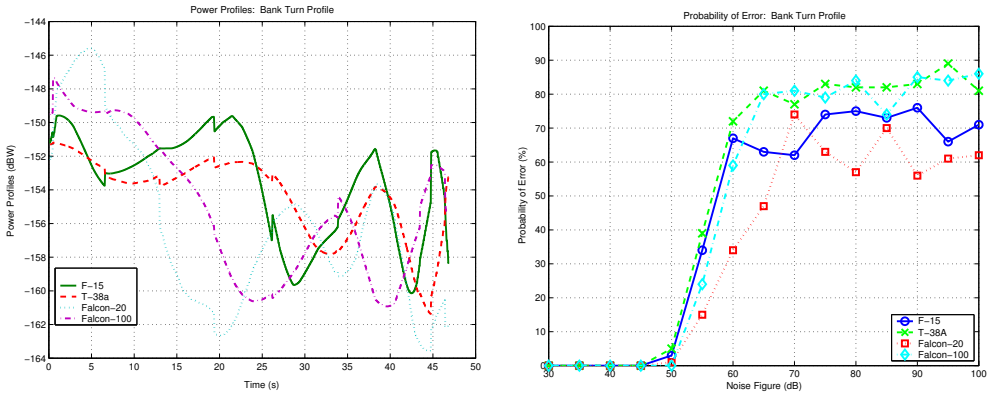

Figure 4. Constant-altitude circular banked turn: a.) power profiles (left), b.) probability of error vs. noise figure (right).

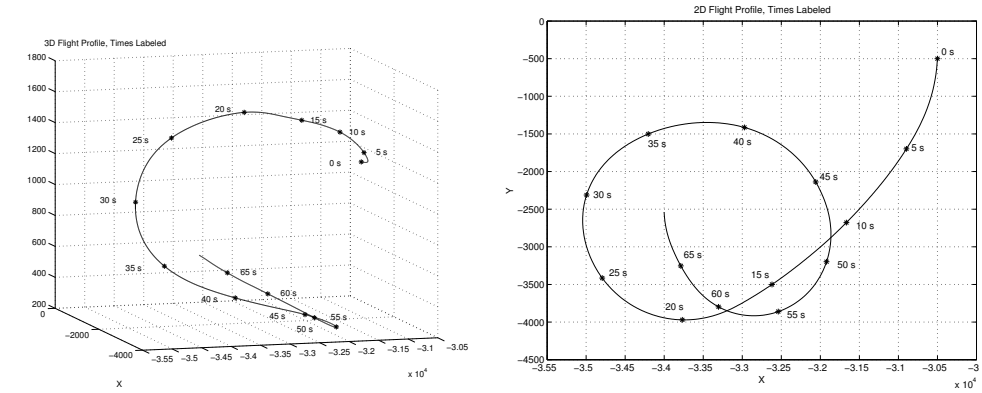

Figure 5. F-15 maneuver: a) 3-D view (left), b) top view (right).

3.4. Edwards Trajectory

To gauge the performance of the algorithm when the target is maneuvering, the third test uses the Edwards trajectory. During the maneuver, the target changes altitudes and executes turns with varying degrees of curvature. This maneuver is shown in Figure 5 from both 3-D and 2-D perspectives, and was previously used to test the coordinated flight model.

To generate a baseline for comparison, this algorithm is first run using the known aircraft orientation angles. This essentially removes the coordinated flight model, and any error it induces, from the process. This test is then redone using the full algorithm, including the coordinated flight model. To simulate the possibility that the position estimates obtained from the passive radar system contain errors, a third test in conducted in which the estimated aircraft position is translated 300 m north and 300 m west. During this final test, the algorithm attempts to recognize targets while assuming these incorrect position estimates are correct.

The power profiles and probability of error curves generated for the F-15 under the three different tests are shown in Figures 6a and 6b, respectively. Although the power profiles show some marked deviations when the orientation angles are estimated and when the position errors are included, the probability of error curves corresponding to the three tests are remarkably similar. In fact, there seems to be little degradation in performance due to using the coordinated flight model, even in the presence of position errors. This is also true for the T-38 and Falcon-100, whose plots are shown in Figures 7 and 8, respectively.

The only aircraft for which degradation in performance is noted is the Falcon-20. Even in this case, the performance is nearly identical when the estimated orientation angles are substituted for the actual ones. The

Table 9. Confusion matrix for the banked turn trajectory with noise figure = 50 dB.

Aircraft	F-15	T-38A	Falcon-20	Falcon-100
F-15	97	3	0	0
T-38A	5	95	0	0
Falcon-20	0	0	99	1
Falcon-100	0	0	0	100

Table 10. Confusion matrix for the banked turn trajectory with noise figure = 60 dB.

Aircraft	F-15	T-38A	Falcon-20	Falcon-100
F-15	33	19	22	26
T-38A	19	28	27	26
Falcon-20	4	9	66	21
Falcon-100	7	13	39	41

Table 11. Confusion matrix for the banked turn trajectory with noise figure = 70 dB.

Aircraft	F-15	T-38A	Falcon-20	Falcon-100
F-15	38	22	23	17
T-38A	36	23	24	17
Falcon-20	32	22	26	20
Falcon-100	33	22	26	19

Table 12. Confusion matrix for the Edwards trajectory with noise figure = 60 dB, using real orientation angles.

Aircraft	F-15	T-38A	Falcon-20	Falcon-100
F-15	98	0	0	2
T-38A	1	94	0	5
Falcon-20	0	0	100	0
Falcon-100	0	6	0	94

Table 13. Confusion matrix for the Edwards trajectory with noise figure = 60 dB, using estimated orientation angles.

Aircraft	F-15	T-38A	Falcon-20	Falcon-100
F-15	97	1	0	2
T-38A	2	90	0	8
Falcon-20	0	0	100	0
Falcon-100	1	17	0	82

Table 14. Confusion matrix for the Edwards trajectory with noise figure = 60 dB, using incorrect position estimates.

Aircraft	F-15	T-38A	Falcon-20	Falcon-100
F-15	100	0	0	0
T-38A	3	86	0	11
Falcon-20	0	1	96	3
Falcon-100	3	18	0	79

Table 15. Confusion matrix for the Edwards trajectory with noise figure = 70 dB, using real orientation angles.

Aircraft	F-15	T-38A	Falcon-20	Falcon-100
F-15	55	20	10	15
T-38A	31	30	21	18
Falcon-20	7	11	75	7
Falcon-100	32	25	21	22

Table 16. Confusion matrix for the Edwards trajectory with noise figure = 70 dB, using estimated orientation angles.

Aircraft	F-15	T-38A	Falcon-20	Falcon-100
F-15	54	16	16	14
T-38A	27	34	22	17
Falcon-20	10	7	80	3
Falcon-100	30	24	21	25

Table 17. Confusion matrix for the Edwards trajectory with noise figure = 70 dB, using incorrect position estimates.

Aircraft	F-15	T-38A	Falcon-20	Falcon-100
F-15	66	17	6	11
T-38A	36	35	13	16
Falcon-20	15	17	60	8
Falcon-100	37	27	13	23

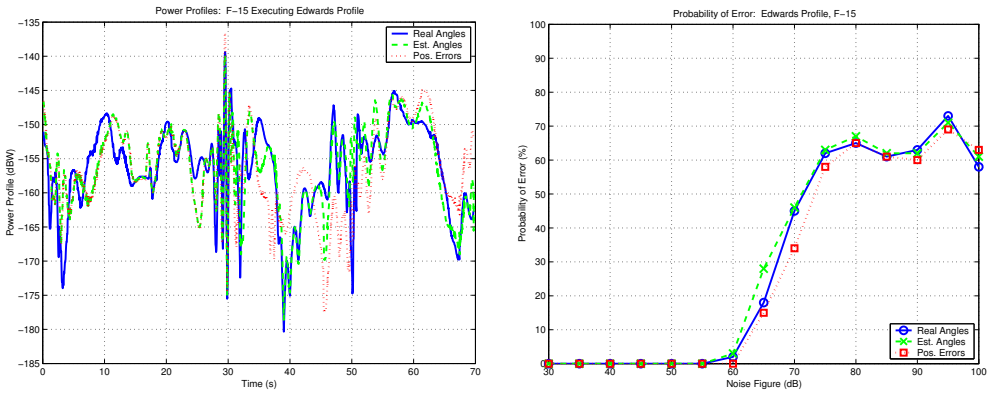

Figure 6. F-15 executing the Edwards trajectory: a) power profiles (left), b) probability of error (right).

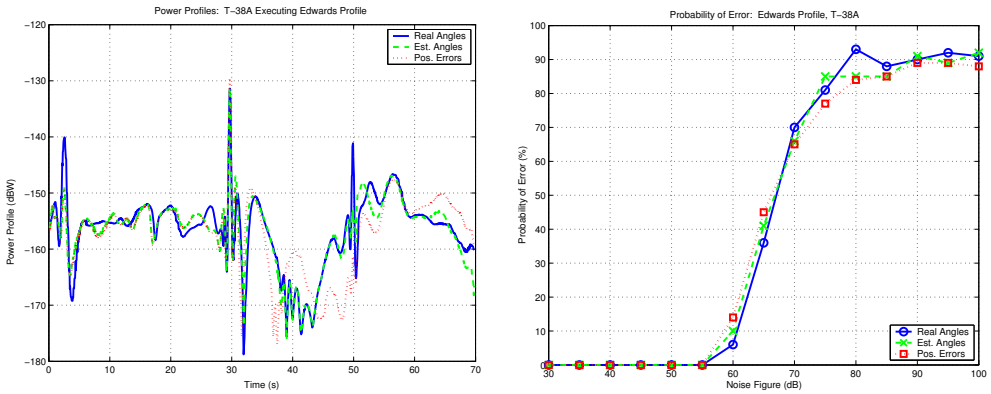

Figure 7. T-38A executing the Edwards trajectory: a) power profiles (left), b) probability of error (right).

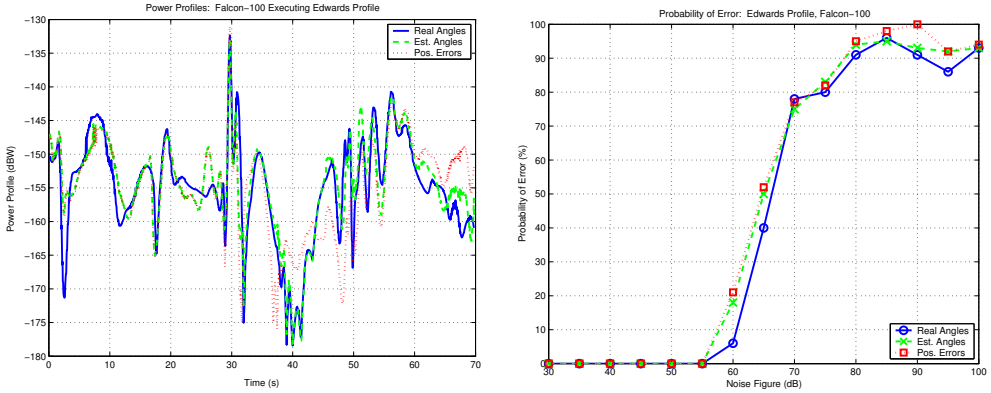

Figure 8. Falcon-100 executing the Edwards trajectory: a) power profiles (left), b) probability of error (right).

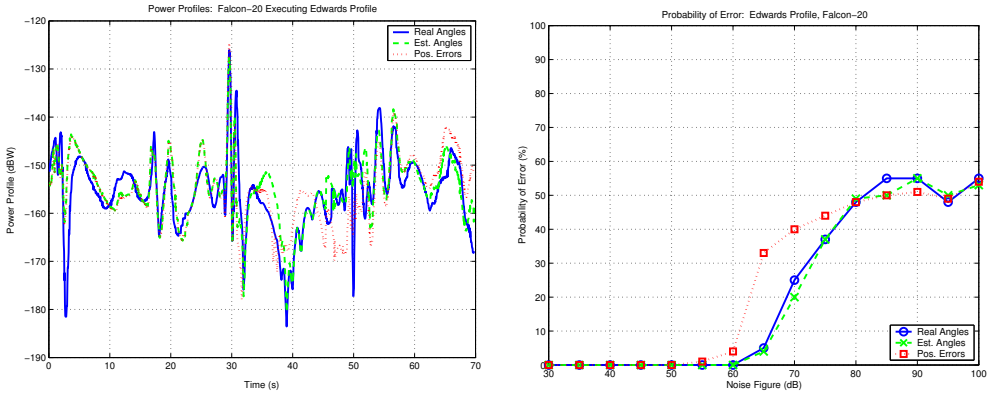

Figure 9. Falcon-20 executing the Edwards trajectory: a) power profiles (left), b) probability of error (right).

only performance degradation occurs when the errant positions are used to estimate the orientation angles. The power profiles and probability of error plots for the Falcon-20 appear in Figure 9.

The confusion matrices obtained with a noise figure of 60 dB are shown in Tables 12 through 14. To get a better sense of the differences in algorithm performance between the three tests, we computed the percentage of total errors. For a noise figure of 60 dB, the algorithm is correct 97% of the time when the orientation angles are known, 92% of the time when the orientation angles are estimated from correct positions, and 90% of the time when incorrect position estimates are used.

Although performance degrades significantly when the noise figure increases to 70 dB, the results of the three tests remain similar to each other. At a noise figure of 70 dB, the algorithm is correct 46% of the time when the correct orientation angles are used, 49% of the time when the estimated orientation angles are used, and 46% of the time when incorrect positions are used to estimate the orientation angles. Confusion matrices corresponding to these three tests are displayed in Tables 15 through 17.

4. SUMMARY

Passive radar is an emerging technology that is only beginning to be exploited by the scientific community. The addition of ATR capabilities can only enhance the effectiveness of these systems. While this task was attempted by Herman with a particle filtering scheme, the major contribution of this paper is that it demonstrates that good results are often possible with a simpler approach.

The results presented in this paper provide a good deal of insight into the viability of this algorithm. Whether the maneuver is simple or complex, for the particular set of targets shown here, the ability to identify the aircraft model is largely dependent upon the maximum signal power being larger than the noise power. If 40 dB is truly a good estimate of the noise figure, then the results obtained using this approach are highly encouraging. Of course, we would not expect a real system to perform exactly as well as our simulations, since there will always be additional effects that cannot be easily modeled.

These results indicate that as long as the targets fall within the receiver's main lobe and are sufficiently close in range, the algorithm will have little trouble identifying them. Performance can then be expected to decline for aircraft whose trajectories do not cross through the receiver's main lobe, or whose position is too far away from the system to generate sufficient SNR. The range required to generate sufficient SNR is itself dependent upon the target type and orientation.

It is worth noting that preliminary finding using the same scenarios and horizontally polarized transmitters and receivers are not as encouraging. Future work will address the differences between the two, and will seek a more robust classification algorithm by jointly estimating target type and orientation. Additional plans for future work also include expansion of the FISC database via sophisticated means.

ACKNOWLEDGMENTS

This work was supported by NATO NC3A and start-up funds from the School of Electrical and Computer Engineering at the Georgia Institute of Technology. The authors would like to thank Dr. Paul Howland and Dr. Rene van der Heiden for their assistance.

REFERENCES

1. S. Jacobs and J. O'Sullivan, "Automatic target recognition using sequences of high resolution radar range-profiles," *IEEE Trans. on Aerospace and Electronic Systems* **36**(2), pp. 364–382, 2000.
2. S. Herman, *A Particle Filtering Approach to Joint Passive Radar Tracking and Target Classification*, Doctoral Dissertation, Department of Electrical and Computer Engineering, Univ. of Illinois at Urbana-Champaign, Urbana, IL, 2002.
3. S. Herman and P. Moulin, "A particle filtering approach to joint radar tracking and automatic target recognition," in *Proc. IEEE Aerospace Conference*, (Big Sky, Montana), March 10-15 2002.
4. Y. Lin and A. Ksienski, "Identification of complex geomtrical shapes by means of low-frequency radar returns," *The Radio and Electronic Engineer* **46**, pp. 472–486, Oct. 1976.

5. H. Lin and A. Ksienski, "Optimum frequencies for aircraft classification," *IEEE Trans. on Aerospace and Electronic Systems* **17**, pp. 656–665, Sept. 1981.
6. J. Chen and E. Walton, "Comparison of two target classification techniques," *IEEE Trans. on Aerospace and Electronic Systems* **22**, pp. 15–21, Jan. 1986.
7. H. Griffiths and N. Long, "Television-based bistatic radar," *IEE Proceedings, Part F* **133**, pp. 649–657, December 1986.
8. P. Howland, "Target tracking using television-based bistatic radar," *IEE Proc. F: Radar, Sonar, and Navigation* **146**, pp. 166–174, June 1999.
9. J. Sahr and F. Lind, "The Manastash ridge radar: A passive bistatic radar for upper atmospheric radio science," *Radio Science* , pp. 2345–2358, Nov.-Dec. 1997.
10. J. Sahr and F. Lind, "Passive radio remote sensing of the atmosphere using transmitters of opportunity," *Radio Science* , pp. 4–7, March 1998.
11. A. Doucet, N. de Freitas, and N. Gordon, *Sequential Monte Carlo Methods in Practice*, Springer-Verlag, 2001.
12. L. Ehrman and A. Lanterman, "Estimation of aircraft orientation from flight paths using a coordinated flight model," *submitted to IEEE Transactions on Aerospace and Electronic Systems* , November 2002.
13. L. Ehrman, *Automatic Target Recognition Using Passive Radar and a Coordinated Flight Model*, Master's Thesis, School of Electrical and Computer Engineering, Georgia Institute of Technology, Atlanta, GA, 2003.
14. D. Mensa, "Radar imaging," *International Journal of Imaging Systems and Technology* **4**, pp. 148–163, 1992.
15. D. Barton, *Modern Radar System Analysis*, Artech House, 1988.
16. M. A. Ringer, G. J. Frazer, and S. J. Anderson, "Waveform analysis of transmitters of opportunity for passive radar," *Surveillance Systems Division, Electronics and Surveillance Research Laboratory* .
17. L. Ehrman and A. Lanterman, "Automated target recogntion using passive radar and coordinated flight models," in *Automatic Target Recognition XIII*, **SPIE Proc. 5094**, (Orlando, FL), April 2003.